CHEMISTRY OF MATERIALS
Cite This: Chem. Mater. XXXX, XXX, XXX−XXX
Article
pubs.acs.org/cm

Electronic Structure of Polymer Dielectrics: The Role of Chemical and Morphological Complexity

Lihua Chen,[†] Rohit Batra,[†] Raghavan Ranganathan,[‡] Gregory Sotzing,[¶] Yang Cao,[§] and Rampi Ramprasad*[,†]

[†]School of Materials Science and Engineering, Georgia Institute of Technology, 771 Ferst Drive NW, Atlanta, Georgia 30332, United States

[‡]Department of Chemical Engineering, Massachusetts Institute of Technology, 25 Ames Street, Cambridge, Massachusetts 02142, United States

[¶]Polymer Program, University of Connecticut, 97 North Eagleville Road, Storrs, Connecticut 06269, United States

[§]Electrical and Computer Engineering, University of Connecticut, 371 Fairfield Way, Storrs, Connecticut 06269, United States

Supporting Information

ABSTRACT: The electronic structure of polymers contains signatures that correlate with their short-term and long-term integrity when subjected to large electric stresses. A detailed picture of the electronic structure of realistic models of polymers has been difficult to obtain, mainly due to the chemical and morphological complexity encountered in polymers. In this work, we have undertaken a comprehensive analysis of the electronic structure of six model polymers displaying chemical and morphological diversity, namely, polyethylene (PE), polypropylene (PP), polystyrene (PS), poly(methyl methacrylate) (PMMA), polyethylene terephthalate (PET), and polybutylene terephthalate (PBT), using first-principles density functional theory computations and classical molecular dynamics simulations. In particular, we have studied the role of monomer chemistry, tacticity, and large-scale morphological disorders in shaping the electronic structure of these polymers. We find that monomer chemistry and morphological disorder cooperate to create localized energy states and the formation of shallow/deep trap depths near the band edges, but tacticity has little effect on the band structure. Appropriate connections and comparisons between the computed results (e.g., band gap and trap depths) and the available experimental data have also been provided. Critical insights on physicochemical and electronic structure relationships are revealed, providing a pathway for understanding the factors that control electrical conduction and degradation of polymers (i.e., charge transport mechanisms, ionization processes, and carrier injections from electrodes).

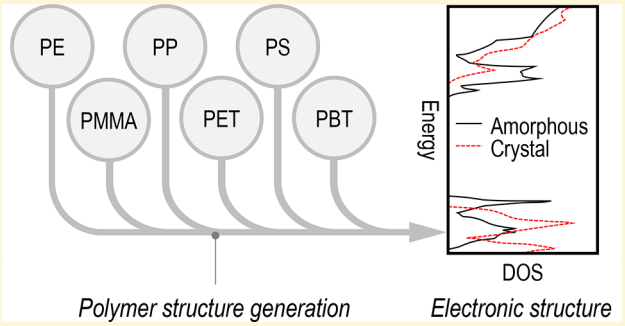

INTRODUCTION

The use of insulating polymers is ubiquitous in electronic and electrical applications, such as high voltage cables,[1−3] film capacitors,[4−7] and field effect transistors.[8,9] This is primarily due to their ease of processing along with their superior electrical properties, such as high resistivity and high breakdown strength. However, with prolonged usage, as part of a working device, the insulating properties of these polymers degrade due to electrical, thermal, or mechanical stresses and eventually result in their dielectric breakdown.[2,10,11]

The electronic structure of polymers (either as prepared or during operation) contains features that correlate with their electrical performance.[2,12] Naturally, the two important attributes that dictate the intrinsic electronic structure of a polymer are its chemical repeat unit and the structural arrangement of its atoms. On the one hand, the large-scale morphological disorders (due to semicrystalline or amorphous phases) present in a polymer can alter its electronic structure by introducing band tail energy states, band edge position shifts, and band gap reductions. Consequently, these alterations will reduce the ionization energy and the band offsets at the electrode/polymer interface, overall, leading to enhanced charge transport within the polymer and increased charge injection at the electrode/polymer interface.[2,12,13] On the other hand, the presence of certain functional groups within the polymer repeat unit or the occurrence of impurities (e.g., C═O) in polyethylene (PE) can provide additional localized band states, which serve as trapping centers for the charges/excitons and thus support additional channels for carrier conduction. Carrier transport and recombination could initiate bond breakage within the polymer, thereby leading to new defects and the corresponding new defect states and,

Received: July 15, 2018
Revised: October 16, 2018
Published: October 17, 2018

DOI: 10.1021/acs.chemmater.8b02997
Chem. Mater. XXXX, XXX, XXX−XXX

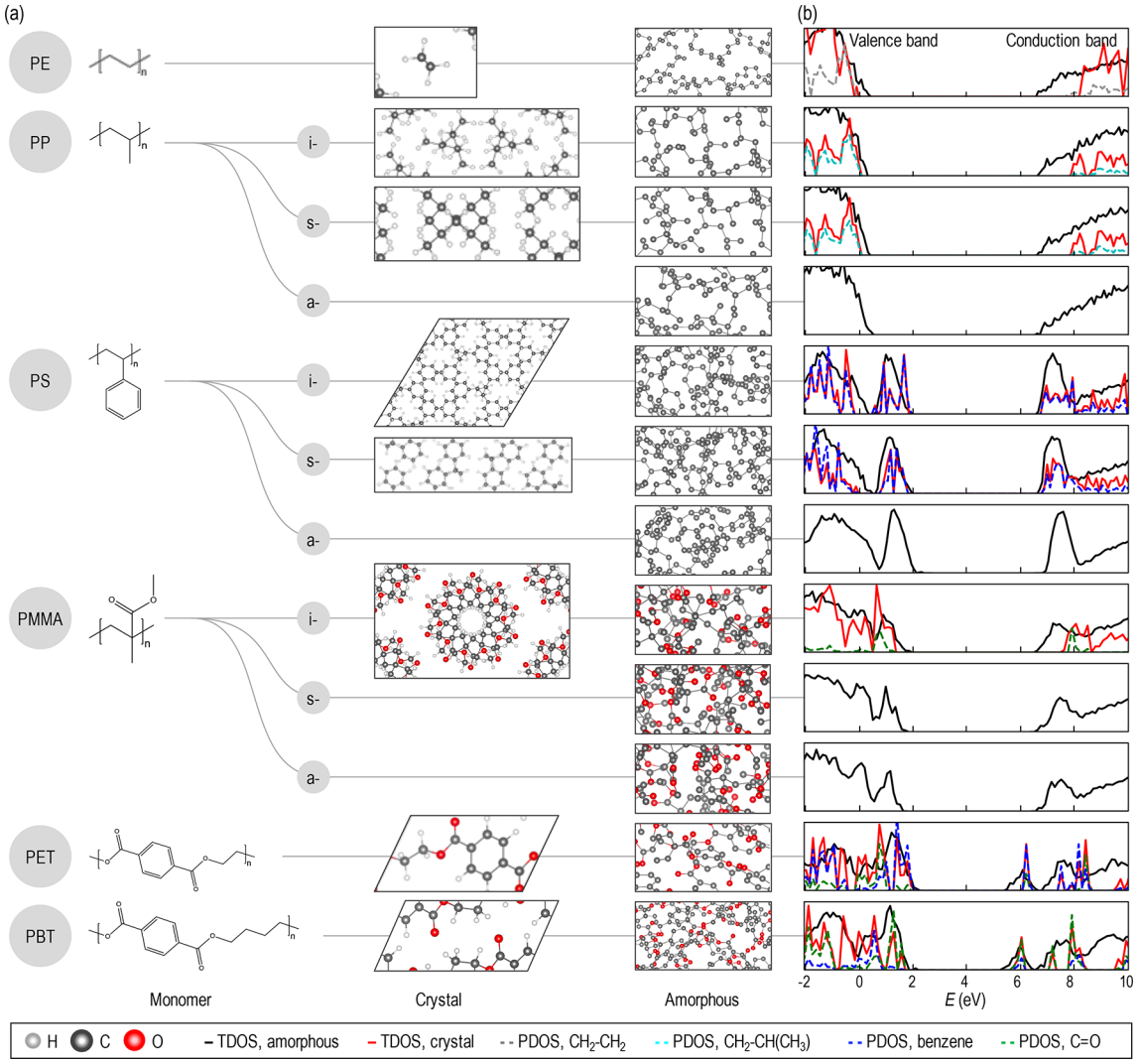

Figure 1. Relationship between the physicochemical and the electronic structures of six model polymers. (a) Structures of the monomers and the crystalline and the amorphous phases of the polymers considered, with the different tacticities (i.e., isotactic (i-), syndiotactic (s-), and atactic (a-)). We note that the tacticity information for certain crystalline polymers is unknown and only the local backbone structure of amorphous phases is shown. The C, H, and O atoms are denoted by gray, white, and red spheres, respectively. (b) The total electronic density of states (TDOS) and the projected density of states (PDOS) corresponding to CH_2-CH_2, $CH_2-CH(CH_3)$, benzene, and C=O groups in the crystalline phases. The energy levels are with respect to the average C-1*s* core level of the crystalline PE.

hence, additional trapping centers. Thus, a gradual cycle of carrier transport, charge trapping, bond breaking, and formation of new defect states is followed, until the polymer finally suffers a breakdown.[2,12,13] Therefore, a study of the electronic structure and its variation under different relevant conditions is the first step toward developing an understanding of the phenomenon of electrical breakdown in polymers, or materials in general.

Past experimental and computational efforts have attempted to associate the physicochemical structures[14−23] and the electronic properties (e.g., trap depths and band gaps) of polymers,[12,24−34] most notably, for PE.[34−36] The empirical studies primarily involve the use of thermal-luminescences (TL), thermally stimulated current (TSC),[37] thermally stimulated depolarization current, (TSDC)[38] or space charge limited current (SCLC)[12,39] measurements to estimate the trap states induced by the chemical defects or the morphological disorders in the polymer. However, these measurements are, at best, only semiquantitative owing to the chemical and physical complexity of the polymers and the inherent limitations/assumptions of the instrumention techniques employed. While there exist some computational work on the relatively simpler case of PE,[34] a systematic study to identify the relationship between the physicochemical and electronic structures of model polymers, including polypropylene (PP), polystyrene (PS), poly(methyl methacrylate) (PMMA), polyethylene terephthalate (PET), and polybutylene terephthalate (PBT), is still missing. Again, the primary reason is the difficulty to accurately model the large-scale complex structures of these polymers using a first-principles approach.

In this work, we attempt to fill this gap and provide a comprehensive picture of the electronic structure (see Figure 1) of the six chemically diverse model polymers, i.e., PE, PP, PS, PMMA, PET, and PBT, using consistent and systematic density functional theory (DFT) computations and classical molecular dynamics (MD) simulations. In particular, we study the effect of monomer chemistry, tacticity, and large-scale morphological disorders (involving 1700−2600 atoms) on the

DOI: 10.1021/acs.chemmater.8b02997
Chem. Mater. XXXX, XXX, XXX−XXX

electronic structure of these polymers. Our findings suggest that chemical variations in the polymer repeat unit can significantly modulate its band edges and drastically shift the band offsets at the polymer−electrode interface, thereby, considerably affecting the electric conduction within a polymer. Likewise, the large-scale morphological variations or disorders were found to degrade the electronic structure, introducing "trap" states within the band gap. Appropriate comparisons with experimental results have been made to quantitatively establish the trap depths in these polymers. Furthermore, the identified trap depths can serve as useful inputs to phenomenological or mesoscale polymer charge transport models. The present contribution provides a pathway to understand the features that control electrical conduction and degradation in polymers.

MODEL POLYMER STRUCTURES AND COMPUTATIONAL DETAILS

Model Polymer Structures. Both crystalline and amorphous phases, each with three possible variations in tacticity, i.e., isotactic (i-), syndiotactic (s-), or atactic (a-), were modeled for the aforementioned six polymers considered in this work. Some crystalline cases in which the polymer either does not display a certain tacticity type or the corresponding structural parameters are unknown were not considered. With these cases removed, the crystalline phases (shown in Figure 1a) investigated include PE, i-PP (α phase), s-PP, i-PS, s-PS, i-PMMA, PET, and PBT (α phase). In the case of amorphous phases, however, all three tacticity variations were explored. Each of these amorphous structures was generated via classical MD simulations of a supercell containing 4 polymeric chains, each consisting of 100, 50, 40, 40, 20, and 20 monomers (see Figure 1a) for the case of PE, PP, PS, PMMA, PET, and PBT, respectively. Further, each chain was terminated with H atoms.

We note that, while many polymers, such as PE and PP, display semicrystalline nature, we chose to study the two extreme situations comprising pure crystalline and pure amorphous phases. Thus, the results provided in this study can be interpolated for such polymers depending on their degree of crystallinity. In addition, we note that the polymer-chain lengths considered here are reasonably long to capture numerous morphological disorders present in polymers. Therefore, only minor deviations in the electronic structure are expected when these systems are modeled with larger chain lengths. For example, the difference between the band gap of amorphous PE with 100 monomers and 200 monomers[34] is just 0.2 eV.

Computational Details. *General Computational Scheme.* All DFT calculations were performed using the Vienna *Ab-Initio* Simulation Package (VASP),[40] with the Perdew−Burke−Ernzerhof (PBE) exchange-correlation (XC) functional and the projector-augmented wave method.[41] A plane-wave energy cutoff E_{cut} of 400 eV was applied and the Monkhorst−Pack k-point meshes[42] for each system are summarized in Table S1 of Supporting Information (SI). vdW-DF2 functional was used for van der Waals interactions,[43−45] which are deemed important for polymers.[46,47] Starting from the geometries based on empirical structural parameters, the crystalline cases were first relaxed using DFT (PBE functional) to obtain equilibrium structures with atomic forces less than 0.01 eV/Å. These relaxed structures were then used to compute the crystalline band gap values with the hybrid XC functional (HSE06).[48] For the amorphous phases, however, the relaxed structures obtained from MD simulations were directly used to estimate the band gap owing to the large system size.

To generate the amorphous phases of the polymers, classical MD simulations based on the OPLS-AA force field[49] were carried out using the LAMMPS simulation package[50] with a time-step of 1 fs. The melt and quench method was adopted in which first, an NVT simulation at T = 600 K was performed for 1 ns, followed by an NPT simulation (P = 1 atm and T = 600 K) for 5 ns. The obtained liquid phases were then cooled from 600 to 300 K using an NPT ensemble for 1 ns. The resulting solid phases were further equilibrated over 5 ns using a NPT simulations (at T = 300 K). In NVT and NPT simulations, Nose-Hoover thermostat and barostat were applied.[51,52] Finally, five representative configurations were randomly selected from the equilibrated MD trajectories (from the last 10 ps) for the electronic structure calculations. The rational behind adopting this sampling procedure has been provided in the SI using the example case of PE and PBT.

Electronic Structure Calculations. While the electronic structures of all crystalline phases were computed using the HSE06 XC functional,[48] for large-scale amorphous structures, an estimate of the electronic structure at the HSE06 level was made in the following manner. First, a single-point PBE calculation was performed for the given structure. The resulting PBE-level conduction band minimum (CBM) and E_g values were then corrected using the linear regression models (with correlation coefficient, $R^2 > 0.97$) given in eqs 1 and 2, respectively. These models are based on the PBE- and HSE06-levels CBM and E_g results for about 250 polymers and molecules (consisting of C, H, O elements),[53] as shown in Figure S1 of the SI. On the other hand, due to the poor correlation between the PBE- and the HSE06-level valence band maximum (VBM) values, the VBM results were computed based on the energy difference between E_{CBM}^{HSE06} and E_g^{HSE06}.

$$E_g^{HSE06} = 1.140 \times E_g^{PBE} + 0.799, \quad R^2 = 0.97 \tag{1}$$

$$E_{CBM}^{HSE06} = 1.028 \times E_{CBM}^{PBE} - 0.423, \quad R^2 = 0.98 \tag{2}$$

To compare electronic structure results across diverse polymers, the 1s core level states of carbon atoms in model polymers were computed using the initial state approximation as implemented in VASP. Kohn−Sham eigenvalues were then corrected by aligning the average 1s core level states of all carbon atoms (excluding C atoms in the C═O group), with respect to those of the perfect bulk PE. To estimate the CBM, VBM, and E_g for the amorphous phases, an average over the values obtained from the five selected configurations were performed. To further elucidate the contributions from specific functional groups toward the electronic structure of crystalline polymers, its projected DOS (PDOS) was computed.

RESULTS AND DISCUSSION

Physical Structures. Figure 1a shows the known crystal structures of the selected polymers. The polymers PE, s-PP, s-PS, and i-PMMA display orthorhombic phases, consisting of two $-[CH_2-CH_2]-$, two $-[(CH_2-CH(CH_3)]_4-$, four $-[(CH_2-CH(C_6H_5)]_2-$, and four $-[(CH_2-C(CH_3)-(C_2O_2H_3)]_5-$ chains, respectively. On the other hand, i-PP, i-PS, and PET and PBT exhibit monoclinic, hexagonal, and triclinic symmetries, respectively. Again, these phases consist of

DOI: 10.1021/acs.chemmater.8b02997
Chem. Mater. XXXX, XXX, XXX−XXX

Table 1. Structural Parameters of Crystalline Phases of Different Polymers, As Computed Using DFT[a]

polymer	method	a (Å)	b (Å)	c (Å)	α (deg)	β (deg)	γ (deg)	ρ (g/cm^3)
PE	DFT	6.79	4.70	2.56	90	90	90	1.14
	expt.	7.12	4.85	2.55	90	90	90	1.05
i-PP (α)	DFT	6.32	18.64	6.51	90	99.92	90	1.11
	expt.	6.67	20.8	6.5	90	98.67	90	0.94
s-PP	DFT	5.08	7.16	13.86	90	90	90	1.11
	expt.	5.6	7.4	14.5	90	90	90	0.93
i-PS	DFT	20.83	20.83	6.55	90	90	120	1.26
	expt.	21.9−22.1	21.9−22.1	6.65−6.63	−	−	−	1.11−1.13
s-PS	DFT	8.31	29.79	5.12	90	90	90	1.13
	expt.	8.81	28.82	5.06	90	90	90	1.11
i-PMMA	DFT	19.04	11.13	10.58	93.6	90	90	1.49
	expt.	20.98	12.06	10.40	90	90	90	1.26
PET	DFT	4.58	5.98	10.40	97.3	116.6	112.8	1.46
	expt.	4.56	5.96	10.75	98.5	112	111.5	1.50
PBT (α)	DFT	4.31	5.64	11.70	100.0	115.6	110.4	1.65
	expt.	4.86	5.96	11.65	99.7	116	110.8	1.40

[a]For comparison, the corresponding experimental values[22] are also provided.

four $-[CH_2-CH(CH_3)]_3-$, six $-[CH_2-CH(C_6H_5)]_3-$, one $-[C_{10}H_8O_4]-$, and one $-[C_{12}H_{12}O_4]-$ chains, resepectively. We also note that i-PP, i-PS, and i-PMMA have 3/1, 3/1, and 10/1 (double) helical structures,[24,25] respectively, which are known to have higher conformational stability compared to their respective all-trans chains. The structural parameters of these phases are summarized in Table 1, along with the respective experimental values.[22] A good agreement between the theoretical and experimental results is evident.

The pure amorphous phases of polymers, generated using the classical MD simulations, are also shown in Figure 1a. Because of the isotropic nature of the amorphous structures, only a segment of the supercell illustrating the local backbone structure is shown. The corresponding radial distribution functions and dihedral angle distributions are provided in Figures S2 and S3 of the SI, which demonstrate that no long-range periodicity is present in the amorphous phases and reasonable structures (bond length and dihedral angles) were obtained. In addition, the obtained physical densities of polymers are summarized in Table 2 and match well with the past theoretical[14−21] and experimental[22,23] values at 300 K. Moreover, for all polymers, the physical densities were found to be almost independent of the tacticity of the amorphous phase. To characterize conformational disorders of polymer chains, the average order parameter (P_2) was computed using eq 1 of the SI.[54] From the equation it can be derived that P_2 ranges from 1 to 0 for the extreme cases of purely parallel and randomly oriented (amorphous) polymer chains, respectively. For the polymers considered, the P_2 (see Table 2) was found to range from 0.34−0.56, indicating that numerous morphological disorders are included in the generated amorphous phases. Among all cases considered, s-PS was found to have the highest P_2 value owing to its high crystalline nature.

Table 2. Physical Properties, i.e., Density and Order Parameter (P_2), of Amorphous Phases

		density (g/cm^3)			
polymer	tacticity	this work	others' work	expt. (300 K)	P_2
PE		0.86	0.85−0.86[a]	0.85[h]	0.51
PP	i-	0.85			0.48
	s-	0.85		0.85−0.86[h]	0.44
	a-	0.85	0.89[b]		0.48
PS	i-	1.00			0.46
	s-	1.00		1.04−1.07[h]	0.56
	a-	1.01	1.01[c], 1.05[d]		0.45
PMMA	i-	1.11	1.16[e], 1.23[f]		0.43
	s-	1.10	1.19[f]	1.17−1.20[h]	0.47
	a-	1.09			0.44
PET		1.25	1.26−1.30[g]	1.34[i]	0.41
PBT		1.18	−	−	0.34

[a]References 14 and 15. [b]Reference 16. [c]Reference 17. [d]Reference 18. [e]Reference 19. [f]Reference 20. [g]Reference 21. [h]Reference 22. [i]Reference 23.

Electronic Structure. Figure 1b presents the computed total electronic density of states (TDOS) for the different crystalline (red color) and amorphous (black color) phases of polymers considered in this work. The calculated band gap of crystalline (E_g^{cry}) and the corrected band gap of amorphous (E_g^{amor}) phases are summarized in Table 3, along with the reported empirical measurements.[26,55−57] For E_g^{amor}, the average value of five selected configurations considered for

Table 3. Band Gap of Crystalline (E_g^{cry}) and Amorphous (E_g^{amor}) Phases of Polymers Considered in This Work, Given in eV

polymer	tacticity	E_g^{cry}	E_g^{amor}	expt.
PE		8.28	6.30 ± 0.03	8.80[a,b]; 6.9[c]
PP	i-	7.86	6.41 ± 0.07	
	s-	7.54	6.34 ± 0.08	8.40[a,d]; 7.0[c]
	a-	−	6.30 ± 0.10	
PS	i-	4.90	4.75 ± 0.08	
	s-	5.14	4.85 ± 0.04	4.4[c]
	a-	−	4.74 ± 0.09	
PMMA	i-	6.30	4.77 ± 0.10	
	s-	−	5.00 ± 0.14	5.2, 5.6[e]
	a-	−	5.00 ± 0.25	
PET		4.17	3.36 ± 0.13	4.0[c]
PBT		4.07	3.43 ± 0.16	−

[a]High crystallinity. [b]Reference 26. [c]Reference 55. [d]Reference 56. [e]Reference 57.

DOI: 10.1021/acs.chemmater.8b02997
Chem. Mater. XXXX, XXX, XXX−XXX

each system is shown, with the standard deviation within ±0.25 eV. As expected, the theoretical E_g^{cry} values of PE and PP match best with the respective experimental measurements (8.8 and 8.4 eV) made on the highly crystalline samples. However, due to the semicrystalline nature of the commercially available PE, PP, and PET samples, the reported experimental band gaps (i.e., 6.9, 7.0, and 4.0 eV, respectively) lie somewhere between the two theoretical extremes of E_g^{cry} and E_g^{amor}. PS and PMMA, on the other hand, mostly exist in the amorphous phase and the experimental values agree well with the respective computed values of E_g^{amor}. Overall, two important trends can be established using Figure 1b and Table 3: (1) the band gaps of the six polymers follow the order PE ∼ PP > PMMA > PS > PET ∼ PBT, and (2) the band gaps of amorphous phases are consistently lower than that of the corresponding crystalline phases. These results clearly indicate that the monomer chemistry and the morphological disorders drastically modulate the electronic structure of a polymer, as discussed in detail next.

Role of Monomer Chemistry. In order to understand the effects of different functional groups on the electronic structure of polymers, the projected DOS (PDOS) of the relevant groups are shown in Figure 1b as dashed lines. Based on the PDOS of CH_2−CH_2 in PE and CH_2−$CH(CH_3)$ in PP, it can be seen that the valence band edge of these polymers is determined by the sp^3-hybridized σ bonding orbitals, while the conduction band edge is controlled by the σ^* antibonding orbitals. Further, the CH_3 branches in PP slightly decrease the overlap of σ bonding orbitals, leading to lower E_g^{cry} values, in contrast to that of PE. However, such effects are negligible when comparing the amorphous phases of these polymers due to the dominant effect from conformational disorder.

In the case of PS, PMMA, PET, and PBT, localized energy states are introduced by the functional groups present in the monomers. For example, in PS, the six sp^2-hybridized carbon atoms within the phenyl group form three π bonding and three π^* antibonding orbitals, which make the valence and the conduction band edges, respectively (see blue dashed lines in Figure 1b). In the case of PMMA, the PDOS analysis (green dashed lines) reveals that the band edges are controlled by the C═O functional groups. While the nonbonding orbitals (from O lone-pair electrons) constitute the valence band edges, the conduction band edges are from the $\pi^*_{C=O}$ antibonding orbitals. As a result, PS and PMMA have relatively lower band gap than that of PE and PP. However, between PS and PMMA, the former has a lower band gap due to delocalization of π bonding and π^* antibonding orbitals of the phenyl group. These findings can also be extended to understand the source of band edges in PET and PBT. The combination of benzene with C═O group results in further delocalization of the π orbitals and thus the lowest band gap in the case of PET and PBT. Simply put, the higher the conjugation of the π orbitals, the lower the band gap of the polymer.

Role of Morphology/Conformation. Next, we study the effect of structural arrangement or morphology on the electronic structure of a polymer. It is evident from Figure 1b that the conduction (valence) band edge of the amorphous phase is consistently lower (higher) than the respective crystalline value. These additional energy states, introduced within the band gap, serve as the centers for electron (E_t^e) and hole (E_t^h) trap depths, which are quantitatively reproduced in Table 4. Available experimental values are also provided, which are believed to be electron trap depths.[12,37−39,58] In the case of amorphous PE and PP, our results indicate introduction of shallow hole and deep electron trap depths, which is consistent with the available experimental values.[12,39] While the former is caused by the conformational disorder in the polymer chains, the latter is due to the low physical density (0.85 g/cm^3, as opposed to ≃1.1 g/cm^3 for the crystalline phase) of the amorphous phase that substantially increases interchain distances and thus reduces the hybridization of the antibonding orbitals discussed earlier.

Table 4. Additional Electron (E_t^e) and Hole (E_t^h) Trap Depths (in eV) Present in Amorphous Phases, with Respect to Their Crystalline Phases[a]

polymer	tacticity	E_t^h	E_t^e	expt.
PE		0.32	1.66	0.8−1.4[b]
PP	i-	0.27	1.17	
	s-	0.07	1.13	0.5−0.7[c]
	a-	0.36	1.19	
PS	i-	0.02	0.14	
	s-	0.03	0.27	0.05−0.45[d]
	a-	0.05	0.11	
PMMA	i-	0.40	1.12	
	s-	0.34	0.96	0.65−0.88[e]
	a-	0.33	0.97	
PET		0.18	0.62	0.2−0.4[c]; 0.33, 0.76[f]
PBT		0.27	0.37	−

[a]Experimental values are believed to be electron trap depths. [b]Reference 12. [c]Reference 39. [d]Reference 58. [e]Reference 38. [f]Reference 37.

In the case of PS, the shallow E_t^e of 0.11−0.26 eV can be attributed to the low conformational freedom available due to the presence of the phenyl groups. The computed electron trap depth is close to the TL-based measurements of 0.08−0.45 eV.[58] For PMMA, PET, and PBT, the contributions to E_t^h and E_t^e can be traced back to the presence of additional O═C—O—C conformations in the amorphous phase. While O═C—O—C dihedral angles range from 60° to 120° in the amorphous phase, these have a value of 0° in the crystalline phase. Because of the higher concentration and the higher conformational freedom associated with the O═C—O—C groups, deep trap depths (of about 1 eV) are introduced in PMMA, which is close to the β relaxation of the O═C—O—C group measured by the TSDC at 50 °C.[38] For PET and PBT, however, shallow trap depths were obtained. This is consistent with the results derived from SCLC spectroscopy (0.2−0.4 eV)[39] and TSC (0.33, 0.76 eV)[37] measurements in the case of PET. We further note that tacticity has a negligible effect on the band structure of the amorphous phases. This can be explained by the isotropic physical properties (i.e., densities and order parameters) obtained for the different cases considered, as shown in Table 2.

Implications. Several important trends and insights can be made using the results shown in Figure 1 and Tables 3 and 4. First, decreasing crystallinity (or increasing amorphous phase) of the polymers enhances their charge transport via introduction of trap levels near the band edges. In the case of PE and PP, conformational disorder in the amorphous phases was found to induce shallow trap depths, assisting hole transport by the trapping/detrapping process. Similarly, the electron transport was found to be substantially enhanced by the formation of deep electron trap depths (1.1−1.7 eV) near the conduction band owing to the low density of the

DOI: 10.1021/acs.chemmater.8b02997
Chem. Mater. XXXX, XXX, XXX−XXX

amorphous phase. Likewise, morphological disorder in the polymer chains of PS, PMMA, PET, and PBT was found to enhance both the hole and the electron transport. While shallow electron and hole trap depths were obtained in PS and PBT, suggesting increased electrical conduction due to trapping/detrapping processes, deep electron trap depths were found in PMMA and PET because of the orientational freedom of the O═C—O—C groups. This is expected to enhance the electron transport mechanism via trap-assisted band conduction.

Second, the trapping levels introduced due to the low crystallinity (or the amorphous phase) of the polymer can drastically reduce the electron injection barrier height from the electrode to the polymer—i.e., the energy differences between the Fermi level of the metal electrode and the band edges of the polymer. Based on our past work,[34] the Fermi level of Al electrode is estimated to be around 4 eV. Thus, qualitatively, the electron/hole barrier heights of PS, PMMA, PET, and PBT are likely to be lower than that of PE and PP. Particularly, these barriers heights are expected to be lowest in the case of PET and PBT. However, empirical measurements of the amount of charge accumulated in these polymers have been found to follow the trend PET < PS ∼ PP < PE.[59] This inconsistency could be because of the opposite internal field induced from the trapped charge near the electrode−polymer interface. The localized energy states in the band edges of PS, PMMA, PET, and PBT (see Figure 1b) would promote higher trapped charge density near the interface, thereby reducing the net electric field within the polymer. Moreover, for polymers, such as PMMA, PET and PBT, the polar O═C—O functional group can further lower the net electric field owing to its alignment with the external electric field.[60] Therefore, while the intrinsic injection barrier height maybe be small, the initial trapped charge can have a "protective" effect by deterring the injection of additional carriers, overall resulting in a low charge accumulation within the polymer. This is also the reason why PET is used as a space charge suppression layer between the metal electrode and the PE film.[3]

Third, Figure 1 shows that the valence band edges of PS, PMMA, PET, and PBT are higher than that of PE and PP, resulting in lower ionization energies, i.e., the energy differences between the valence band maximum and the vacuum level, for the former four polymers. This observation indicates that the impact ionization process is more relevant in the case of PS, PMMA, PET, and PBT, assisting electron multiplication via collisions between the hot electrons and the functional groups (e.g., C═O), and thus encouraging the process of an electron avalanche.[2,10,11] Furthermore, the resulting active radicals can initiate a series of chemical reactions, forming new defects and hence more trap states. All these complex processes culminate in the dielectric breakdown of the polymer.

Finally, we note that a large amount of physical and electronic structure data has been generated as part of this work that covers a diverse range of model polymers. The data may be mined and utilized using machine learning techniques to either identify additional hidden correlations or to train force fields for MD simulations.[61−63] This can help advance the past data-driven and high-throughput computational work that has led to important polymer discoveries.[5−7,53,64−67] All data that have emerged from the present work is made available in our online repository https://khazana.gatech.edu.

SUMMARY

The electronic structure of six model polymers, including PE, PP, PS, PMMA, PET, and PBT, has been comprehensively investigated using density functional theory and classical molecular dynamics. The effects of monomer chemistry, tacticity, and large-scale morphological disorders (amorphous phase) on the electronic structure of these polymers have been established, with the results justified based on the projected density of states of the relevant monomer functional groups. While the monomer chemistry was found to introduce localized energy states, the morphological disorder lead to the formation of shallow and deep trap depths near the band edges of the polymer. Tacticity, on the other hand, was found to have relatively little effect on the band structure. Theoretical predictions of polymer band gaps and conformation induced trap depths were found to be in agreement with the available experimental measurements and can serve as vital inputs to large-scale mesoscale/phenomenological charge transport models. Finally, the derived correlations between the physicochemical and the electronic structures of polymers are critical to understand the electrical conduction mechanism in polymers. All these contributions can help to understand the degradation and breakdown behavior within polymers and to provide a pathway toward rational design of breakdown-resistant polymer dielectrics.

ASSOCIATED CONTENT

Supporting Information

The Supporting Information is available free of charge on the ACS Publications website at DOI: 10.1021/acs.chemmater.8b02997.

Computational details: primary parameters in DFT calculations; order parameters calculations; electronic structure calculations. Physical structures characterization: radial distribution function and dihedral angle distributions of crystalline and amorphous phases of six model polymers. Validation of the sampling procedure of amorphous phases (PDF)

AUTHOR INFORMATION

Corresponding Author

*(R.R.) E-mail: rampi.ramprasad@mse.gatech.edu.

ORCID

Lihua Chen: 0000-0002-9852-8211
Rohit Batra: 0000-0002-1098-7035
Yang Cao: 0000-0001-7034-2792
Rampi Ramprasad: 0000-0003-4630-1565

Notes

The authors declare no competing financial interest.

ACKNOWLEDGMENTS

This work is supported by the Office of Naval Research through Grants N00014-17-1-2656 and N00014-16-1-2580. Computational support was provided by the Extreme Science and Engineering Discovery Environment (XSEDE). The authors thank Chiho Kim for assistances with the creation of all the figures.

REFERENCES

(1) Dadbin, S.; Frounchi, M.; Saeid, M. H.; Gangi, F. Molecular structure and physical properties of E-beam crosslinked low-density

DOI: 10.1021/acs.chemmater.8b02997
Chem. Mater. XXXX, XXX, XXX−XXX

polyethylene for wire and cable insulation applications. *J. Appl. Polym. Sci.* **2002**, *86*, 1959−1969.
(2) Dissado, L. A.; Fothergill, J. C. *Electrical Degradation and Breakdown in Polymers*; IET: London, UK, 1992.
(3) Mazzanti, G.; Marzinotto, M. *Extruded cables for high-voltage direct-current transmission: advances in research and development*; John Wiley & Sons: Hoboken, NJ, USA, 2013; Vol. *93*.
(4) Chu, B.; Zhou, X.; Ren, K.; Neese, B.; Lin, M.; Wang, Q.; Bauer, F.; Zhang, Q. A dielectric polymer with high electric energy density and fast discharge speed. *Science* **2006**, *313*, 334−336.
(5) Sharma, V.; Wang, C.; Lorenzini, R. G.; Ma, R.; Zhu, Q.; Sinkovits, D. W.; Pilania, G.; Oganov, A. R.; Kumar, S.; Sotzing, G. A.; et al. Rational design of all organic polymer dielectrics. *Nat. Commun.* **2014**, *5*, 4845−4853.
(6) Huan, T. D.; Boggs, S.; Teyssedre, G.; Laurent, C.; Cakmak, M.; Kumar, S.; Ramprasad, R. Advanced polymeric dielectrics for high energy density applications. *Prog. Mater. Sci.* **2016**, *83*, 236.
(7) Mannodi-Kanakkithodi, A.; Treich, G. M.; Huan, T. D.; Ma, R.; Tefferi, M.; Cao, Y.; Sotzing, G. A.; Ramprasad, R. Rational Co-Design of Polymer Dielectrics for Energy Storage. *Adv. Mater.* **2016**, *28*, 6277−6291.
(8) Yoon, M.-H.; Yan, H.; Facchetti, A.; Marks, T. J. Low-voltage organic field-effect transistors and inverters enabled by ultrathin cross-linked polymers as gate dielectrics. *J. Am. Chem. Soc.* **2005**, *127*, 10388−10395.
(9) Roberts, M. E.; Queraltó, N.; Mannsfeld, S. C.; Reinecke, B. N.; Knoll, W.; Bao, Z. Cross-linked polymer gate dielectric films for low-voltage organic transistors. *Chem. Mater.* **2009**, *21*, 2292−2299.
(10) Martinez-Vega, J. *Dielectric materials for electrical engineering*; John Wiley & Sons: Hoboken, NJ, U.S.A., 2013.
(11) Ieda, M. Dielectric breakdown process of polymers. *IEEE Trans. Electr. Insul.* **1980**, *EI-15*, 206−224.
(12) Ieda, M. Electrical conduction and carrier traps in polymeric materials. *IEEE Trans. Electr. Insul.* **1984**, *EI-19*, 162−178.
(13) Kao, K. C. Electrical conduction and breakdown in insulating polymers. Presented at IEEE International Conference on Properties and Applications of Dielectric Materials (ICPADM), 2000; pp 1−17.
(14) Moyassari, A.; Unge, M.; Hedenqvist, M. S.; Gedde, U. W.; Nilsson, F. First-principle simulations of electronic structure in semicrystalline polyethylene. *J. Chem. Phys.* **2017**, *146*, 204901.
(15) Wang, Y.; MacKernan, D.; Cubero, D.; Coker, D. F.; Quirke, N. Single electron states in polyethylene. *J. Chem. Phys.* **2014**, *140*, 154902.
(16) Mansfield, K. F.; Theodorou, D. N. Molecular dynamics simulation of a glassy polymer surface. *Macromolecules* **1991**, *24*, 6283−6294.
(17) Tatek, Y. B.; Tsige, M. Structural properties of atactic polystyrene adsorbed onto solid surfaces. *J. Chem. Phys.* **2011**, *135*, 174708.
(18) Ayyagari, C.; Bedrov, D.; Smith, G. D. Structure of Atactic Polystyrene: A Molecular Dynamics Simulation Study. *Macromolecules* **2000**, *33*, 6194−6199.
(19) Sane, S. B.; Çağin, T.; Knauss, W. G.; Goddard, W. A., III Molecular dynamics simulations to compute the bulk response of amorphous PMMA. *J. Comput.-Aided Mater. Des.* **2001**, *8*, 87−106.
(20) Tung, K.-L.; Lu, K.-T. Effect of tacticity of PMMA on gas transport through membranes: MD and MC simulation studies. *J. Membr. Sci.* **2006**, *272*, 37−49.
(21) Wang, Q.; Keffer, D. J.; Petrovan, S.; Thomas, J. B. Molecular Dynamics Simulation of Poly(ethylene terephthalate) Oligomers. *J. Phys. Chem. B* **2010**, *114*, 786−795.
(22) Mark, J. *Polymer Data Handbook*; Oxford University Press: Oxford, U.K., 2009.
(23) Thompson, A.; Woods, D. Density of amorphous polyethylene terephthalate. *Nature* **1955**, *176*, 78.
(24) Tadokoro, H. Structure and properties of crystalline polymers. *Polymer* **1984**, *25*, 147−164.
(25) Kusanagi, H.; Chatani, Y.; Tadokoro, H. The crystal structure of isotactic poly (methyl methacrylate): packing-mode of double stranded helices. *Polymer* **1994**, *35*, 2028−2039.
(26) Less, K. J.; Wilson, E. G. Intrinsic photoconduction and photoemission in polyethylene. *J. Phys. C: Solid State Phys.* **1973**, *6*, 3110.
(27) Laurent, C.; Teyssedre, G.; Le Roy, S.; Baudoin, F. Charge dynamics and its energetic features in polymeric materials. *IEEE Trans. Dielectr. Electr. Insul.* **2013**, *20*, 357−381.
(28) Bamji, S.; Bulinski, A.; Abou-Dakka, M. Luminescence and space charge in polymeric dielectrics-[whitehead memorial lecture (2008)]. *IEEE Trans. Dielectr. Electr. Insul.* **2009**, *16*, 1376.
(29) Teyssedre, G.; Tardieu, G.; Laurent, C. Characterisation of crosslinked polyethylene materials by luminescence techniques. *J. Mater. Sci.* **2002**, *37*, 1599−1609.
(30) Chen, L.; Huan, T. D.; Quintero, Y. C.; Ramprasad, R. Charge injection barriers at metal/polyethylene interfaces. *J. Mater. Sci.* **2016**, *51*, 506−512.
(31) Chen, L.; Tran, H. D.; Wang, C.; Ramprasad, R. Unraveling the luminescence signatures of chemical defects in polyethylene. *J. Chem. Phys.* **2015**, *143*, 124907.
(32) Wang, C.; Pilania, G.; Boggs, S.; Kumar, S.; Breneman, C.; Ramprasad, R. Computational strategies for polymer dielectrics design. *Polymer* **2014**, *55*, 979−988.
(33) Stournara, M.; Ramprasad, R. A first principles investigation of isotactic polypropylene. *J. Mater. Sci.* **2010**, *45*, 443.
(34) Chen, L.; Huan, T. D.; Ramprasad, R. Electronic Structure of Polyethylene: Role of Chemical, Morphological and Interfacial Complexity. *Sci. Rep.* **2017**, *7*, 6128.
(35) Huzayyin, A.; Boggs, S.; Ramprasad, R. Density functional analysis of chemical impurities in dielectric polyethylene. *IEEE Trans. Dielectr. Electr. Insul.* **2010**, *17*, 926−930.
(36) Huzayyin, A.; Boggs, S.; Ramprasad, R. Quantum mechanical studies of carbonyl impurities in dielectric polyethylene. *IEEE Trans. Dielectr. Electr. Insul.* **2010**, *17*, 920−925.
(37) Kryszewski, M.; Kasica, H.; Patora, J.; Piotrowski, J. Relationship between electric conductivity, thermally stimulated currents, thermoluminescence and polymer structure. *J. Polym. Sci., Part C: Polym. Symp.* **1970**, *30*, 243−259.
(38) Namouchi, F.; Jilani, W.; Guermazi, H. Thermally stimulated depolarization current and dielectric spectroscopy used to study dipolar relaxations and trap level distribution in PMMA polymer. *J. Non-Cryst. Solids* **2015**, *427*, 76−82.
(39) Li, Z.; Uehara, H.; Ramprasad, R.; Boggs, S.; Cao, Y. Density of bulk trap states in polymeric films. Presented at IEEE Conference on Electrical Insulation and Dielectric Phenomena (CEIDP), 2016; pp 1041−1044.
(40) Kresse, G.; Furthmüller, J. Efficient iterative schemes for ab initio total-energy calculations using a plane-wave basis set. *Phys. Rev. B: Condens. Matter Mater. Phys.* **1996**, *54*, 11169.
(41) Perdew, J. P.; Burke, K.; Ernzerhof, M. Generalized gradient approximation made simple. *Phys. Rev. Lett.* **1996**, *77*, 3865.
(42) Monkhorst, H. J.; Pack, J. D. Special points for Brillouin-zone integrations. *Phys. Rev. B* **1976**, *13*, 5188.
(43) Dion, M.; Rydberg, H.; Schröder, E.; Langreth, D. C.; Lundqvist, B. I. Van der Waals Density Functional for General Geometries. *Phys. Rev. Lett.* **2004**, *92*, 246401.
(44) Román-Pérez, G.; Soler, J. M. Efficient Implementation of a van der Waals Density Functional: Application to Double-Wall Carbon Nanotubes. *Phys. Rev. Lett.* **2009**, *103*, 096102.
(45) Klimeš, J. c. v.; Bowler, D. R.; Michaelides, A. Van der Waals density functionals applied to solids. *Phys. Rev. B: Condens. Matter Mater. Phys.* **2011**, *83*, 195131.
(46) Liu, C.-S.; Pilania, G.; Wang, C.; Ramprasad, R. How Critical Are the van der Waals Interactions in Polymer Crystals? *J. Phys. Chem. A* **2012**, *116*, 9347−9352.
(47) Pham, T. H.; Ramprasad, R.; Nguyen, H.-V. Density-functional description of polymer crystals: A comparative study of recent van der Waals functionals. *J. Chem. Phys.* **2016**, *144*, 214905.

DOI: 10.1021/acs.chemmater.8b02997
Chem. Mater. XXXX, XXX, XXX−XXX

(48) Heyd, J.; Scuseria, G. E.; Ernzerhof, M. Hybrid functionals based on a screened Coulomb potential. *J. Chem. Phys.* **2003**, *118*, 8207.
(49) Robertson, M. J.; Tirado-Rives, J.; Jorgensen, W. L. Improved Peptide and Protein Torsional Energetics with the OPLS-AA Force Field. *J. Chem. Theory Comput.* **2015**, *11*, 3499−3509.
(50) Plimpton, S. Fast Parallel Algorithms for Short-Range Molecular Dynamics. *J. Comput. Phys.* **1995**, *117*, 1−19.
(51) Posch, H. A.; Hoover, W. G.; Vesely, F. J. Canonical dynamics of the Nosé oscillator: Stability, order, and chaos. *Phys. Rev. A: At., Mol., Opt. Phys.* **1986**, *33*, 4253−4265.
(52) Hoover, W. G.; Holian, B. L. Kinetic moments method for the canonical ensemble distribution. *Phys. Lett. A* **1996**, *211*, 253−257.
(53) Huan, T. D.; Mannodi-Kanakkithodi, A.; Kim, C.; Sharma, V.; Pilania, G.; Ramprasad, R. A polymer dataset for accelerated property prediction and design. *Sci. Data* **2016**, *3*, 160012.
(54) Brayton, A. L.; Yeh, I.-C.; Andzelm, J. W.; Rutledge, G. C. Vibrational Analysis of Semicrystalline Polyethylene Using Molecular Dynamics Simulation. *Macromolecules* **2017**, *50*, 6690−6701.
(55) Ohki, Y.; Fuse, N.; Arai, T. Band gap energies and localized states in several insulating polymers estimated by optical measurements. Presented at IEEE Conference on Electrical Insulation and Dielectric Phenomena (CEIDP), 2010; pp 1−4.
(56) Xie, H.; Wu, X.; Peng, Z.; Zhang, H. The energy criterion for breaking chemical bonds in electrical breakdown process of polymers. Presented at IEEE International Conference on Properties and Applications of Dielectric Materials (ICPADM), 1994; pp 39−41.
(57) Al-Kadhemy, M. F. H.; Saeed, A. A.; Khaleel, R. I.; Al-Nuaimi, F. J. K. Effect of gamma ray on optical characteristics of (PMMA/PS) polymer blends. *J. Appl. Phys.* **2017**, *11*, 201−207.
(58) Pender, L.; Fleming, R. Thermoluminescence in polystyrene. *J. Phys. C: Solid State Phys.* **1977**, *10*, 1571.
(59) Nagasawa, K.; Honjoh, M.; Takada, T.; Miyake, H.; Tanaka, Y. Electric Charge Accumulation in Polar and Non-Polar Polymers under Electron Beam Irradiation. *IEEJ. Trans. Fundam. Mater.* **2010**, *130*, 1105−1112.
(60) Neagu, E.; Dias, C. Charge injection/extraction at a metal-dielectric interface: experimental validation. *IEEE Electr. Insul. M.* **2009**, *25*, 15−22.
(61) Huan, T. D.; Batra, R.; Chapman, J.; Krishnan, S.; Chen, L.; Ramprasad, R. A universal strategy for the creation of machine learning-based atomistic force fields. *NPJ. Comput. Mater.* **2017**, *3*, 37.
(62) Botu, V.; Batra, R.; Chapman, J.; Ramprasad, R. Machine learning force fields: construction, validation, and outlook. *J. Phys. Chem. C* **2017**, *121*, 511−522.
(63) Botu, V.; Ramprasad, R. Learning scheme to predict atomic forces and accelerate materials simulations. *Phys. Rev. B: Condens. Matter Mater. Phys.* **2015**, *92*, 094306.
(64) Mannodi-Kanakkithodi, A.; Chandrasekaran, A.; Kim, C.; Huan, T. D.; Pilania, G.; Botu, V.; Ramprasad, R. Scoping the polymer genome: A roadmap for rational polymer dielectrics design and beyond. *Mater. Today* **2018**, *21*, 785−796.
(65) Mannodi-Kanakkithodi, A.; Huan, T. D.; Ramprasad, R. Mining Materials Design Rules from Data: The Example of Polymer Dielectrics. *Chem. Mater.* **2017**, *29*, 9001−9010.
(66) Baldwin, A. F.; Huan, T. D.; Ma, R.; Mannodi-Kanakkithodi, A.; Tefferi, M.; Katz, N.; Cao, Y.; Ramprasad, R.; Sotzing, G. A. Rational design of organotin polyesters. *Macromolecules* **2015**, *48*, 2422−2428.
(67) Kim, C.; Chandrasekaran, A.; Huan, T. D.; Das, D.; Ramprasad, R. Polymer Genome: A Data-Powered Polymer Informatics Platform for Property Predictions. *J. Phys. Chem. C* **2018**, *122*, 17575−17585.

DOI: 10.1021/acs.chemmater.8b02997
Chem. Mater. XXXX, XXX, XXX−XXX